Electronic structure and x-ray magnetic circular dichroism in Fe_3O_4 and Mn-, Co-, or Ni-substituted Fe_3O_4

V. N. Antonov* and B. N. Harmon
Ames Laboratory, Iowa State University, Ames, Iowa 50011

A. N. Yaresko
Max-Planck Institute for the Chemical Physics of Solids, Nöthnitzer Strasse 40, D-01187 Dresden, Germany
(Received 24 May 2002; revised manuscript received 19 August 2002; published 22 January 2003)

The electronic structure of charge-ordered magnetite (Fe_3O_4) below the Verwey transition and Mn-, Co-, or Ni-substituted Fe_3O_4 are investigated theoretically from first principles, using the fully relativistic Dirac linear muffin-tin orbital band-structure method. The electronic structure is obtained with the local spin-density approximation (LSDA), as well as with the so-called LSDA+U approach, for which the charge ordering is found to be a stable solution in contrast to a metallic state given by the LSDA. The x-ray absorption spectra as well as the x-ray magnetic circular dichroism spectra at the K, $L_{2,3}$, and $M_{2,3}$ edges for transition metal sites are calculated. A good agreement between theory and experiment is obtained.

DOI: 10.1103/PhysRevB.67.024417 PACS number(s): 71.28.+d, 71.20.−b, 75.30.Mb

I. INTRODUCTION

In recent years, the investigation of magneto-optical effects in the soft x-ray range has gained great importance as a tool for the investigation of magnetic materials.[1] First considered as a rather exotic technique, magnetic x-ray dichroism (MXD) has now developed as an important measurement technique for local magnetic moments. The x-ray magnetic circular dichroism (XMCD) enables a quantitative determination of spin and orbital magnetic moments,[2] element-specific imaging of magnetic domains,[3] and polarization analysis.[4] Motivated by the developing interest in obtaining element-specific magnetic-moment information provided by the XMCD measurements, we have calculated the electronic structure and the XMCD spectra for strongly correlated Fe_3O_4 as well as for the Mn-, Co-, and Ni-substituted Fe_3O_4.

Fe_3O_4 is ferrimagnetically ordered below a high transition temperature ($\sim$850 K). The valency of various atoms is described by the formal chemical formula, $Fe_A^{3+}[Fe^{2+}Fe^{3+}]_B(O^{2-})_4$. The tetrahedral lattice sites (A sites) in the inverse spinel structure are occupied by Fe^{3+} ions, whereas the octahedral lattice sites (B sites) are occupied alternately by equal numbers of Fe^{2+} and Fe^{3+}. At $T_V=120$ K, Fe_3O_4 undergoes a first-order metal-insulator phase transition (Verwey transition).[5,6] The Verwey transition is characterized by an abrupt increase in the electrical conductivity by two orders of magnitude on heating through T_V.[7] Verwey and co-workers[5,8] were the first to point out that this transition is associated with an electron localization-delocalization transition. The Fe^{2+} ion can be regarded as an ''extra'' electron plus an Fe^{3+} ion. When all B sites are equivalent, the extra electron is moves between Fe_B^{3+} ions and the system is a mixed valent metal, with average Fe_B valence, $Z=2.5$. The Verwey phase transition below T_V is accompanied by long-range charge ordering of Fe^{3+} and Fe^{2+} ions on $B1$ and $B2$ sites of the B sublattice. As to how these charges arrange themselves has been the subject of debate[6] since Verwey first proposed that below T_V, all Fe_B^{3+} and Fe_B^{2+} sit on different chains.[5]

The electronic structure of Fe_3O_4 has been investigated experimentally by means of soft x-ray spectroscopy,[9–11] Seebeck-effect measurements,[12] photoelectron spectroscopy,[13–19] optical[20,21] and magneto-optical[22–26] (MO) spectroscopies, and by magnetic dichroism.[27,28]

Energy-band-structure calculations for Fe_3O_4 in the high-temperature cubic phase have been presented in Refs. 29 and 30 in the local spin-density approximation (LSDA). The LSDA band-structure calculations gave only a metallic solution without charge ordering with partially filled bands (containing one electron per two B sites). The energy-band structure for charge ordering in the low-temperature phase of Fe_3O_4 has been calculated in Ref. 31 using the linear muffin-tin orbital (LMTO) method in the LSDA+U approximation. Recently, we performed a theoretical investigation of the electronic structure, optical and magneto-optical spectra of charge-ordered magnetite below the Verwey transition and Mg^{2+}- and Al^{3+}- substituted Fe_3O_4 in LSDA and LSDA+U approximations.[32] The LSDA+U calculations give a reasonably good agreement between theoretically calculated and experimentally measured optical and MO spectra of Fe_3O_4. Since the optical and MO spectra provide information on the transition between the occupied and empty states, it is of interest to investigate the XMCD spectra that provide more information about the energy positions of the upper Hubbard bands of strongly correlated Fe d states in magnetite.

The interpretation of the experimental XMCD spectra of Fe_3O_4 is very difficult due to the existence of three kinds of iron atoms, i.e., Fe_B^{2+}, Fe_B^{3+}, and Fe_A^{3+}. The substitution for one of the types of iron ions by another transition-metal ion provides a possibility for distinguishing transitions from various sites. There are several such experimental studies in the literature. Koide and co-workers reported the XMCD spectra at the Fe $M_{2,3}$ and Co $M_{2,3}$ core-absorption edges in

Fe_3O_4 and $CoFe_2O_4$.[28] For Fe_3O_4, the $M_{2,3}$ prethreshold MCD spectra were measured above and below the Verwey transition temperature. The work by van der Laan *et al.*[33] reported the XMCD spectra at the Ni $L_{2,3}$ edges of $NiFe_2O_4$ (trevorite). The Ni $L_{2,3}$-edge magnetic circular dichroism measurements of ferrimagnetic $Zn_xNi_{1-x}Fe_2O_4$ ($x=0.0$, 0.26, 0.50, and 0.75) were reported by Pong *et al.*[34] Magnetic circular dichroism is reported for $Mn_{2/3}Zn_{1/3}Fe_2O_4$ ferrite in Ref. 35 with the measurements performed on the $2p$ and $3p$ core levels of Mn and Fe.

With the aim of undertaking a systematic investigation of the trends in the transition-metal oxides, we have investigated the electronic structure, spin and orbital magnetic moments, and XMCD spectra of the series Fe_3O_4, $CoFe_2O_4$, $NiFe_2O_4$, and $MnFe_2O_4$. We calculated the XAS (x-ray absorption spectra) and XMCD spectra at K, $L_{2,3}$, and $M_{2,3}$ edges for transition-metals sites. The theoretical results are compared with available experimental data.

The article is organized as follows. Section II presents a description of the crystal structure of Fe_3O_4 and the computational details. Section III is devoted to the electronic structure and XMCD spectra of the Fe_3O_4 and Mn-, Co-, and Ni-substituted Fe_3O_4 calculated in the LSDA and LSDA $+U$ approximations. The XMCD calculations are compared to the experimental measurements. Finally, the results are summarized in Sec. IV.

II. CRYSTAL STRUCTURE AND COMPUTATIONAL DETAILS

Above the Verwey transition temperature, Fe_3O_4 crystallizes in the face-centered-cubic inverse spinel structure with two formula units (14 atoms) per primitive cell. The space group is $Fd\bar{3}m$ (No. 227). The oxygen atoms form a close-packed face-centered-cubic structure with the iron atoms occupying the interstitial positions. There are two types of interstitial sites both occupied by iron atoms. One site is called the A or $8a$ site, tetrahedrally coordinated by four O^{2-} ions composing a diamond lattice. This site is occupied only by Fe^{3+} ions. Another cation site is called the B or $16d$ site, and is coordinated by six O^{2-} ions forming slightly distorted octahedra, which line up along the $\langle 110\rangle$ axes of the cubic lattice sharing edges. The point symmetry of the B site is $D3d$. In the following, we refer to $b1$ axes or $b1$ chains and $b2$ axes or $b2$ chains. The $b1$ direction is $[1\bar{1}0]$, $b2$ is [110], and the c axis is [001]. All the Fe octahedral or B sites lie on either $b1$ or $b2$ chains. In the disordered high-temperature phase, the B sites are occupied by equal numbers of Fe^{2+} and Fe^{3+} ions randomly distributed between $B1$ and $B2$ sites. Below T_V, the system undergoes a first-order transition accompanied by long-range charge ordering of Fe^{3+} and Fe^{2+} ions on the B sites. Verwey from the very beginning proposed a rather simple charge separation: $b1$ chains occupied only by Fe^{2+} ions and $b2$ chains by Fe^{3+} ions (or vice versa).[5] Since that time, the type of charge ordering has been the subject of debate.[6]

Site-preference calculations[36] and neutron-diffraction measurements[37] on bulk systems pointed out that Co^{2+} and Ni^{2+} ions strongly prefer the octahedral B sites while Zn^{2+} ions prefer tetrahedral A sites. However, the results of extended x-ray-absorption fine-structure studies on thin-film $Zn_{0.16}Ni_{0.15}Fe_{2.69}O_4$ show that Ni^{2+} ions occupy both A and B sites with only a preference for B sites.[38] Mn^{2+} ions with the $3d^5$ configuration have almost equal preference for tetrahedral and octahedral positions based on its ionic radii. However, according to Ref. 35, Mn^{2+} ions mostly occupy tetrahedral A sites.

Magneto-optical effects refer to various changes in the polarization state of light upon interaction with materials possessing a net magnetic moment, including rotation of the plane of linearly polarized light (Faraday, Kerr rotation), and the complementary differential absorption of left and right circularly polarized light (circular dichroism). In the near visible spectral range, these effects result from excitation of electrons in the conduction band. Near x-ray absorption edges, or resonances, magneto-optical effects can be enhanced by transitions from well-defined atomic core levels to symmetry selected valence states. There are at least two alternative formalisms for describing resonant soft x-ray MO properties. One uses the classical dielectric tensor.[39] While another uses the resonant atomic scattering factor including charge and magnetic contributions.[40,41] The equivalence of these two descriptions (within the dipole approximation) is demonstrated in Ref. 42.

Using straightforward symmetry considerations, it can be shown that all magneto-optical phenomena (XMCD, MO-Kerr and -Faraday effects) are caused by the symmetry reduction, in comparison to the paramagnetic state, caused by magnetic ordering.[43] Concerning the XMCD properties, this symmetry reduction only has consequences when spin-orbit (SO) coupling is considered in addition. The theoretical description of magnetic dichroism can be cast into four categories. On one hand, there are one-particle (ground-state) and many-body (excited-state) theories; there are also theories for single atoms and those which take into account the solid state. To name a few from each category, for atomic single-particle theories, we refer to Refs. 44 and 45, for atomic many-particle multiplet theory to Refs. 46–49, for solid many-particle theories to Ref. 50, and for solid single-particle theories (photoelectron diffraction) to Refs. 51–54. A multiple-scattering approach to the XMCD, a solid-state one-particle theory, has been proposed by Ebert *et al.*[55–57] and Tamura *et al.*[58]

To calculate the XMCD spectra, one has to account for magnetism and SO coupling at the same time when dealing with the electronic structure of the material considered. Performing band-structure calculations, it is normally sufficient to treat SO coupling in a perturbative way. A more rigorous scheme, however, is obtained by starting from the Dirac equation set up in the framework of relativistic spin-density functional theory.[59] There are quite a few band-structure methods available now that are based on the Dirac equation.[60,61] In one of the schemes, the basis functions are derived from the proper solution of the Dirac equation for the spin-dependent single-site potentials.[62,63] In another one, the basis functions are obtained initially by solving the Dirac

equation without the spin-dependent term and then this term is accounted for in the variational step.[62] In spite of this approximation, the latter scheme gives results in close agreement with the former,[64] while being simpler to implement.

Within the single-particle approximation, the absorption coefficient μ for incident x rays of polarization λ and photon energy $\hbar\omega$ can be determined as the probability of electron transition from an initial core state (with wave function ψ_j and energy E_j) to a final unoccupied state (with wave function $\psi_{n\mathbf{k}}$ and energy $E_{n\mathbf{k}}$)

$$\mu_j^{\lambda}(\omega)=\sum_{n\mathbf{k}} |\langle\Psi_{n\mathbf{k}}|\Pi_{\lambda}|\Psi_j\rangle|^2 \delta(E_{n\mathbf{k}}-E_j-\hbar\omega)\,\theta(E_{n\mathbf{k}}-E_F). \tag{1}$$

Π_{λ} is the dipole electron-photon interaction operator

$$\Pi_{\lambda}=-e\boldsymbol{\alpha}\mathbf{a}_{\lambda}, \tag{2}$$

where $\mathbf{a}_{\lambda}$ is the λ polarization unit vector of the photon potential vector $[a_{\pm}=1/\sqrt{2}(1,\pm i,0), a_z=(0,0,1)]$. (Here, $+/-$ denotes, respectively, left and right circular photon polarizations with respect to the magnetization direction in the solid.) More detailed expressions of the matrix elements for the spin-polarized fully relativistic LMTO method may be found in Refs. 57 and 65.

While the XMCD is calculated using Eq. (1), the main features can be already understood from a simplified expression for paramagnetic solids. With restriction to electric dipole transitions, keeping the integration only inside the atomic spheres (due to the highly localized core sates) and averaging with respect to polarization of the light, one obtains the following expression for the absorption coefficient of the core level with (l,j) quantum numbers:[66]

$$\mu_{lj}^{0}(\omega)=\sum_{l',j'} \frac{2j+1}{4}\left(\frac{\delta_{l',l+1}\delta_{j',j+1}}{j+1}+\frac{\delta_{l',l-1}\delta_{j',j-1}}{j} + \frac{\delta_{l',l+1}\delta_{j',j}}{j(j+1)(2j+1)}\right) N_{l',j'}(E) C_{l,j}^{l',j'}(E) \tag{3}$$

where $N_{l',j'}(E)$ is the partial density of empty states and the $C_{l,j}^{l',j'}(E)$ are the radial matrix elements.[66]

Equation (3) allows only transitions with $\Delta l=\pm 1, \Delta j=0,\pm 1$ (dipole selection rules), which means that the absorption coefficient can be interpreted as a direct measure for the sum of (l,j)-resolved density of states (DOS) curves weighed by the square of the corresponding radial matrix element (which usually is a smooth function of energy). This simple interpretation is valid for the spin-polarized case.[39]

The details of the computational method are described in our previous paper,[32] and here we only mention its several aspects. The electronic structure of the compounds was calculated self-consistently using the local spin-density approximation[67] and the fully relativistic spin-polarized LMTO method in the atomic-sphere approximation, including the combined correction.[60,62,68]

The combined correction terms have been included also in calculation of the matrix elements of Eq. (1).[65] To improve the potential, we include two additional empty spheres in the $16c$, and $48f$ positions. In our band-structure calculations, we neglect the small monoclinic distortion for simplicity. We also adopted the simplest type of charge ordering below T_V, initially proposed by Verwey,[5] namely, we assume that all the Fe_B^{2+} ions are located on $b1$ chains and all the Fe_B^{3+} on $b2$ chains. The basis consisted of the transition metal *s*, *p*, and *d*; O *s*, and *p*, and empty sphere *s*, and *p* LMTO's. The **k**-space integrations were performed with the improved tetrahedron method.[69] For the finite lifetime of the core hole a constant width Γ_c, in general, from Ref. 70, has been used.

We have adopted the LSDA+U method[71] as a different level of approximation to treat the electron-electron correlation. Usually, the Hubbard-like U_{eff} is evaluated by comparison of theoretically calculated energy positions of energy bands with x-ray photoemission spectroscopy and ultraviolet photoemission spectroscopy measurements. It can be also evaluated from the atomic Dirac-Hartree-Fock calculations,[72] Green's-function impurity calculations[73] and from band structure calculations in the super-cell approximation.[74] In our particular case, we have two types of Fe ions in Fe_3O_4 with different occupation numbers for their $3d$ shell. Obviously, the effective repulsion of $3d$ electrons described by U_{eff} depends on the number of holes in the $3d$ shell (the ionicity), and U_{eff} should increase with increasing ionicity.[75] The estimation in Ref. 30 gave the value of the on-site Coulomb interaction parameter for the Fe(B) site equal to 4.1 ± 0.5 eV. Constrained calculations[31] with two types of charge ordering gave $U_{eff}=4.5$ eV. The calculated value of U_{eff} depends on theoretical approximations and for our purposes it is sufficient to regard the value of U_{eff} as a parameter and try to ascertain its value from comparison of the calculated physical properties of Fe_3O_4 with experiments. We found, however, that the optical, MO, and XMCD spectra are rather insensitive to the precise value of U_{eff}. The LSDA+U band-structure calculations with U_{eff} varying from 4 to 6 eV provide the optical, MO, and XMCD spectra in a reasonable agreement with the experimental data. On the other hand, the value of the energy gap strongly depends on the value of U_{eff}. We set the U_{eff} to 4.0 and 4.5 eV for Fe^{2+} and Fe^{3+} ions, respectively. These values give a band gap of 0.19 eV in pure Fe_3O_4.[32] We also set the U_{eff} to 4.0 for Mn^{2+}, Co^{2+}, and Ni^{2+} ions.

The values of orbital magnetic moments were calculated using the modified version of the LSDA+U method, which takes into account that in the presence of the spin-orbit coupling the occupation matrix is not diagonal in spin indices.[76,77]

III. RESULTS AND DISCUSSION

A. Fe_3O_4

The spin-polarized LSDA calculations show[29,30,32] that Fe_3O_4 in the high-temperature phase is a half-metallic ferri-

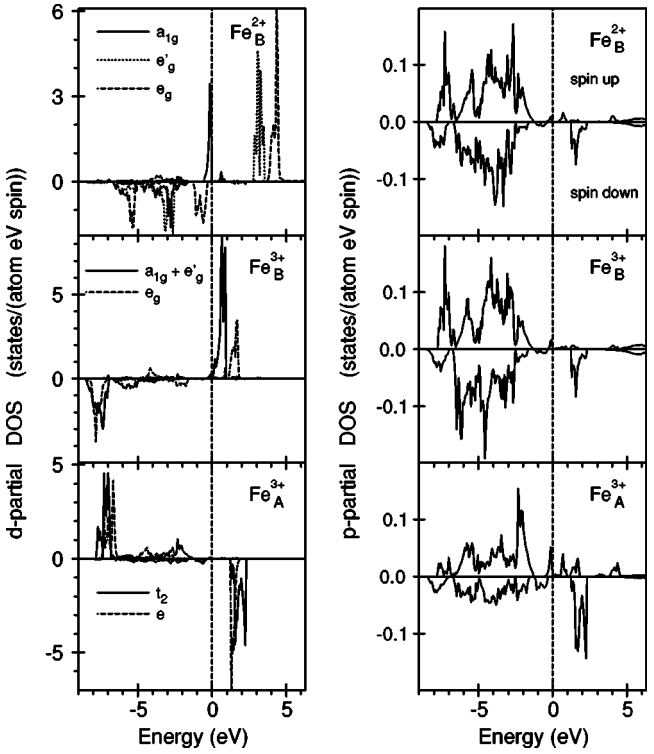

FIG. 1. The LSDA+U partial DOS of Fe_3O_4.

magnet (see Fig. 2 in Ref. 32). The Fermi level crosses only the majority spin energy bands, consisting of spin-up t_{2g} orbitals on the Fe_B sublattice. There is an energy gap for the minority spin bands at the Fermi level. The five d levels of the Fe atom are split due to the crystal field. At the A site (T_d point symmetry) in the spinel structure, the crystal field causes the d orbitals to split into a doublet e ($3z^2-1$ and x^2-y^2) and a triplet t_2 (xy, yz, and xz). The octahedral component of the crystal field at the B site is strong enough that the t_{2g} (xy, yz, and xz) and e_g ($3z^2-1$ and x^2-y^2) orbitals form two separate nonoverlapping bands. At the B site, the crystal field is trigonal ($D3d$), as a result, the t_{2g} orbitals split into singlet a_{1g} and doublet e'_g.

The application of a LSDA calculations to Fe_3O_4 is problematic because of the correlated nature of the d electron in this compound. The intersite Coulomb correlation is well described by the LSDA. However, the on-site Coulomb interaction, which is a driving force for Mott-Hubbard localization, is not well treated within the LSDA. As a result, the LSDA gives only a metallic solution without charge ordering. To take into account the strong on-site d-d electron-electron correlations, we used the LSDA+U method.[71] Figure 1 shows the partial d and p density of states of charge-ordered Fe_3O_4 obtained from the LSDA+U calculation.[32] In contrast to the LSDA, where the stable solution is a metal with a uniform distribution of the $t_{2g\uparrow}$ electrons on the B octahedral sites, the LSDA+U gives a charge-ordered insulator with a direct energy gap value of 0.19 eV at the Γ point. The experimental optical measurements[21] gave a gap of 0.14 eV at $T=10$ K. The energy gap occurs between the Fe_B^{2+} $a_{1g\uparrow}$ (the top of valence band) and Fe_B^{3+} $t_{2g\uparrow}$ (bottom of empty conduction band) states (Fig. 1).

In the charge-ordered magnetite with Fe_B^{2+} and Fe_B^{3+} ions occupying separately the $b1$ and $b2$ chains, the local symmetry is reduced to C_{2v} and C_{2h} at the A and B sites, respectively. The crystal field causes the d orbitals to split into five singlets at each site: a'_1, a''_1, b_1, a_2, and b_2 at the A site and a_{g1}, a_{g2}, a_{g3}, b_{g1}, and b_{g2} at the B site. The tetrahedral component of the crystal field at the A site is strong enough such that the a''_1, a_2 ($3z^2-1$ and x^2-y^2) and a'_1, b_1, and b_2 (the linear combination of the xy, yz, and xz) orbitals form two separate nonoverlapping bands. However, the a''_1-a_2 and a'_1-b_1-b_2 splitting is negligible in comparison with their widths, therefore, we present in Fig. 1 the DOS of e orbitals as a sum of the a''_1 and a_2 orbitals and t_2 as a sum of the a'_1, b_1, and b_2 ones. Correspondingly, at the octahedral B site, we present e_g orbitals as a sum of a_{g3} and b_{g2} orbitals and a'_g as a sum of a_{g2} and b_{g1} ones.

After the consideration of the above band-structure properties, we turn to the XMCD spectra. At the core level edge, XMCD is not only element specific but also orbital specific. For $3d$ transition metals, the electronic states can be probed by the K, $L_{2,3}$, and $M_{2,3}$ x-ray absorption and emission spectra. As pointed out above, Eq. (3) for unpolarized absorption spectra $\mu^0(\omega)$ allows only transitions with $\Delta l=\pm 1, \Delta j=0, \pm 1$ (dipole selection rules). Therefore, only electronic states with an appropriate symmetry contribute to the absorption and emission spectra under consideration. We should mention that in some cases quadruple transitions may play an important role, as it occurs, for example, in rare-earth materials ($2p\rightarrow 4f$ transitions).[78]

Because of the dipole selection rules, apart from the $4s_{1/2}$ states (which have a small contribution to the XAS due to relatively small $2p\rightarrow 4s$ matrix elements[39]) only $3d_{3/2}$ states occur as final states for L_2-XAS for unpolarized radiation, whereas for the L_3-XAS, $3d_{5/2}$ states also contribute. Although, the $2p_{3/2}\rightarrow 3d_{3/2}$ radial matrix elements are only slightly smaller than for the $2p_{3/2}\rightarrow 3d_{5/2}$ transitions the angular matrix elements strongly suppress the $2p_{3/2}\rightarrow 3d_{3/2}$ contribution [see Eq. (3)]. Therefore, in neglecting the energy dependence of the radial matrix elements, the L_2 and the L_3 spectra can be viewed as a direct mapping of the DOS curve for $3d_{3/2}$ and $3d_{5/2}$ character, respectively.

The dichroism at the L_2 and L_3 edges is influenced by the spin-orbit coupling of the initial $2p$-core states. This gives rise to a very pronounced dichroism in comparison with the dichroism at the K edge. In Figs. 2 and 3, the experimentally measured Fe $L_{2,3}$-XMCD spectra[27] in Fe_3O_4 are compared to the theoretical ones calculated within the LSDA and LSDA+U approaches. Two prominent negative minima of Fe L_3-XMCD spectrum are derived from iron ions at octahedral B sites. The major positive maximum is from Fe_A^{3+} ions. In the LSDA+U calculations of the charge-ordered Fe_3O_4, the $L_{2,3}$-XMCD spectra have slightly different shape for the Fe_B^{2+} and Fe_B^{3+} ions. The spectra from the LSDA calculations strongly underestimate the intensity of the first negative minimum (Fig. 2). On the other hand, the LSDA+U calculations correctly reproduce this feature. Although, both the LSDA and LSDA+U calculations are not able to produce

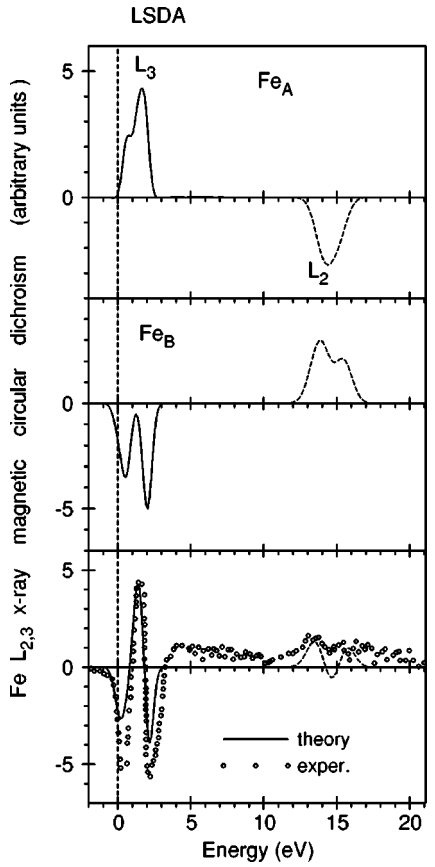

FIG. 2. The Fe $L_{2,3}$-XMCD spectra in Fe_3O_4 calculated with the LSDA method in comparison with the experimental data (circles) (Ref. 27).

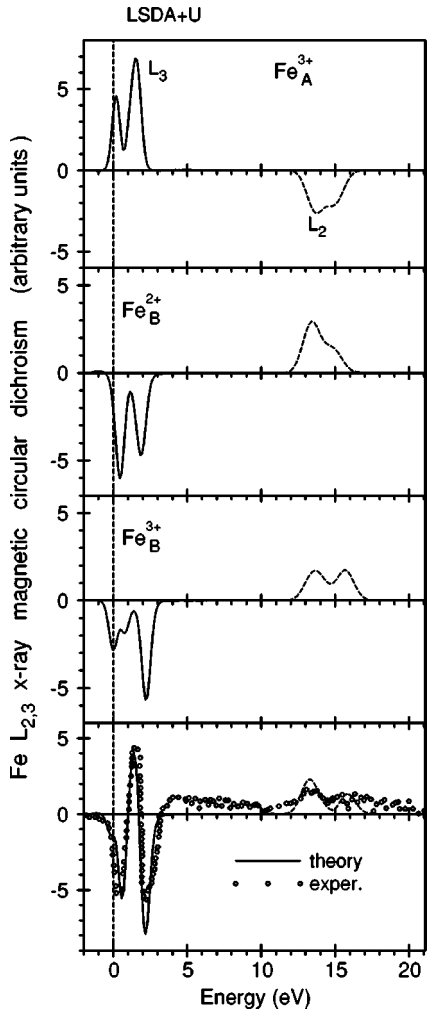

FIG. 3. The Fe $L_{2,3}$-XMCD spectra in Fe_3O_4 calculated with the LSDA+U approximation in comparison with the experimental data (circles) (Ref. 27).

the small positive shoulder at the high-energy side of the main peaks of the Fe L_3-XMCD spectrum.

The XMCD spectra at the $L_{2,3}$ edges are mostly determined by the strength of the SO coupling of the initial $2p$-core states and spin polarization of the final empty $3d_{3/2,5/2}$ states, while the exchange splitting of the $2p$-core states as well as the SO coupling of the $3d$-valence states are of minor importance for the XMCD at the $L_{2,3}$ edge of $3d$-transition metals.[32,39]

To investigate the influence of the initial state on the resulting XMCD spectra, we calculated also the XAS and XMCD spectra of Fe_3O_4 at the $M_{2,3}$ edge. The spin-orbit splitting of the $3p$-core level is about one order of magnitude smaller than for the $2p$-level in Fe_3O_4. As a result, the magnetic dichroism at the $M_{2,3}$ edge is smaller than at the $L_{2,3}$ edge. In addition, the M_2 and M_3 spectra are strongly overlapped and the M_3 spectrum contributes to some extent to the structure of the total $M_{2,3}$ spectrum in the region of the M_2 edge. To decompose a corresponding experimental $M_{2,3}$ spectrum into its M_2 and M_3 parts will, therefore, be quite difficult in general.

In Figs. 4 and 5, the experimentally measured Fe $M_{2,3}$-XMCD spectrum[28] in Fe_3O_4 is compared to the theoretical one calculated within the LSDA and LSDA+U approaches. A better agreement between the theory and the experiment was found when we used the LSDA+U approximation. The LSDA calculations underestimate the intensity of both the prominent negative minima and the second positive maximum at the Fe $M_{2,3}$ edge. In Fe_3O_4, the magnetic moments within the *A* and the *B* sublattices are ferromagnetically aligned while the two sublattices are antiferromagnetic with respect to each other. The XMCD spectra are positive at the M_3 edge and negative at the M_2 edge at the tetrahedral *A* sites and vice versa for the octahedral *B* ones. The interpretation of the experimental Fe $M_{2,3}$-XMCD spectrum is very difficult without a knowledge of the band structure and corresponding optical matrix elements because this spectrum is a superposition of six $M_{2,3}$ spectra (from Fe_A^{3+}, Fe_B^{2+} and Fe_B^{3+} sites) appearing simultaneously in a rather small-energy range.

Figure 6 shows the theoretically calculated Fe *K*-edge XMCD in terms of the difference in absorption $\Delta\mu_K=\mu_K^+-\mu_K^-$ for left and right circularly polarized radiation in Fe_3O_4. Because dipole allowed transitions dominate the absorption spectrum for unpolarized radiation, the absorption coefficient $\mu_K^0(E)$ (not shown) reflects primarily the DOS of unoccupied $4p$-like states $N_p(E)$ of Fe above the Fermi

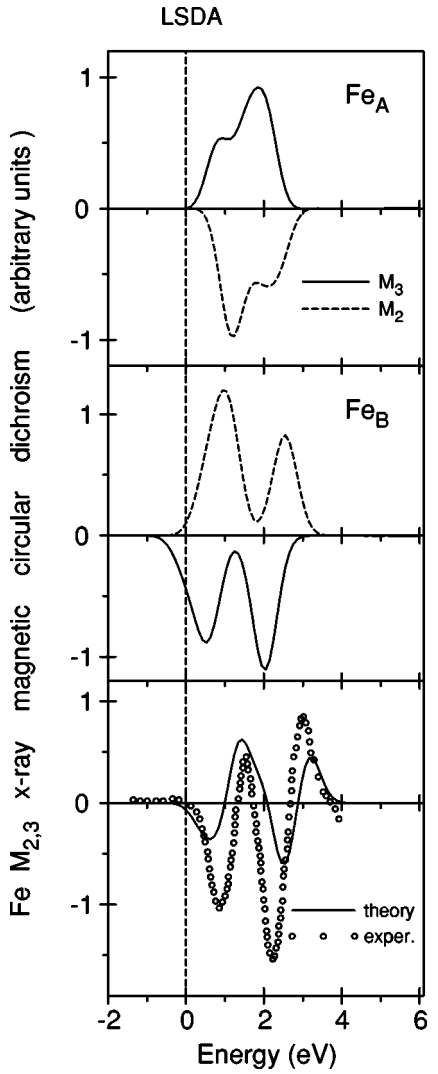

FIG. 4. The Fe $M_{2,3}$-XMCD spectra in Fe_3O_4 calculated with the LSDA method in comparison with the experimental data (circles) (Ref. 28).

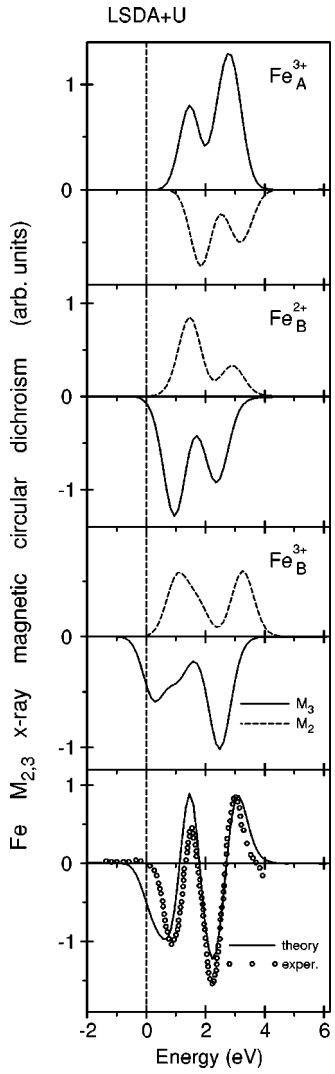

FIG. 5. The Fe $M_{2,3}$-XMCD spectra in Fe_3O_4 calculated with the LSDA+U approximation in comparison with the experimental data (circles) (Ref. 28).

level. Due to the energy-dependent radial matrix element for $1s \rightarrow 4p$ transitions, there is not an exact one-to-one correspondence between $\mu_K(E)$ and $N_p(E)$. The exchange splitting of the initial $1s$-core state is extremely small, therefore, only the exchange and spin-orbit splitting of the final $4p$ states is responsible for the observed dichroism at the K edge. For this reason, the dichroism is found to be very small (Fig. 6). The main contribution to a total XMCD-K spectrum of Fe_3O_4 comes from the Fe_A^{3+} ions.

It was first pointed out by Gotsis and Strange[79] as well as Brooks and Johansson[80] that XMCD-K spectrum reflects the orbital polarization in differential form $d\langle l_z\rangle/dE$ of the p states.

In Fig. 6, we present the K- XMCD spectra, together with a site-dependent function $dm_{tl}(E)$ given by[81]

$$dm_{tl}(E) = \sum_{n\mathbf{k}} \langle \Psi_{tl}^{n\mathbf{k}} | \hat{l}_z | \Psi_{tl}^{n\mathbf{k}} \rangle \delta(E - E_{n\mathbf{k}}), \qquad (4)$$

where $\hat{l}_z$ is the z projection of the angular momentum operator, $E_{n\mathbf{k}}$ and $\Psi_{tl}^{n\mathbf{k}}$ are the energy of the nth band and the part of the corresponding LMTO wave function formed by the states with the angular momentum l inside the atomic sphere centered at the site t, respectively.

In analogy to the l-projected density of states, $dm_{tl}(E)$ can be referred to as the site- and l-projected density of the expectation value of $\hat{l}_z$. This quantity has purely relativistic origins and when the SO interaction is equal to zero $dm_{tl}(E) \equiv 0$. As van Vleck[82] showed for a free ion, the absence of orbital degeneracy is a sufficient condition for the quenching of the orbital moment, which means that the first-order contribution should vanish: $\langle \Psi_{\mathbf{k}} | \hat{l}_z | \Psi_{\mathbf{k}} \rangle = 0$. Thus, $dm_{tl}(E)$ can be considered as the measure of unquenching of the orbital moment due to the SO interaction.

Figure 6 demonstrates that the K- XMCD spectrum and $dm_{tl}(E)$ function are indeed closely related to one another giving a rather simple and straightforward interpretation of the XMCD spectra at the K edge.

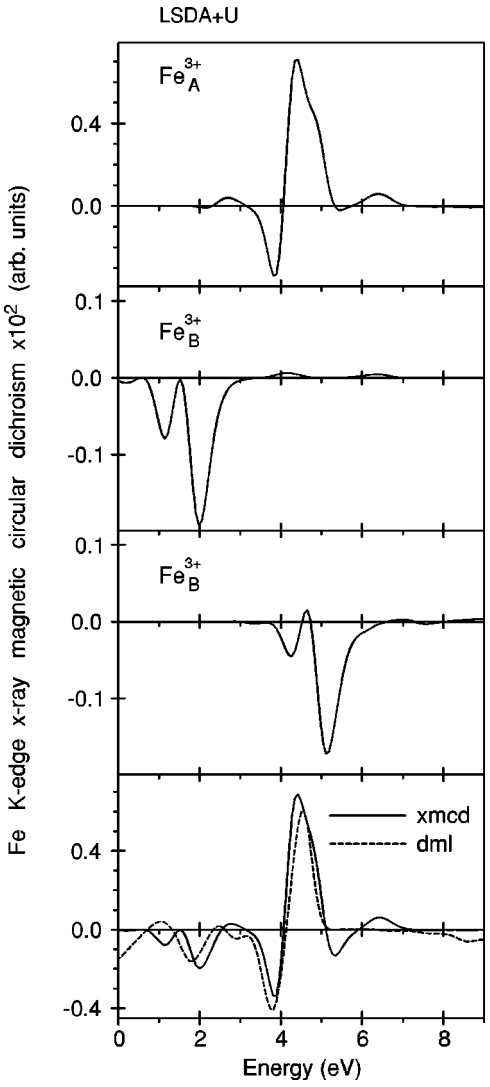

FIG. 6. The Fe *K*-XMCD spectra in Fe_3O_4 calculated with the LSDA+*U* approximation.

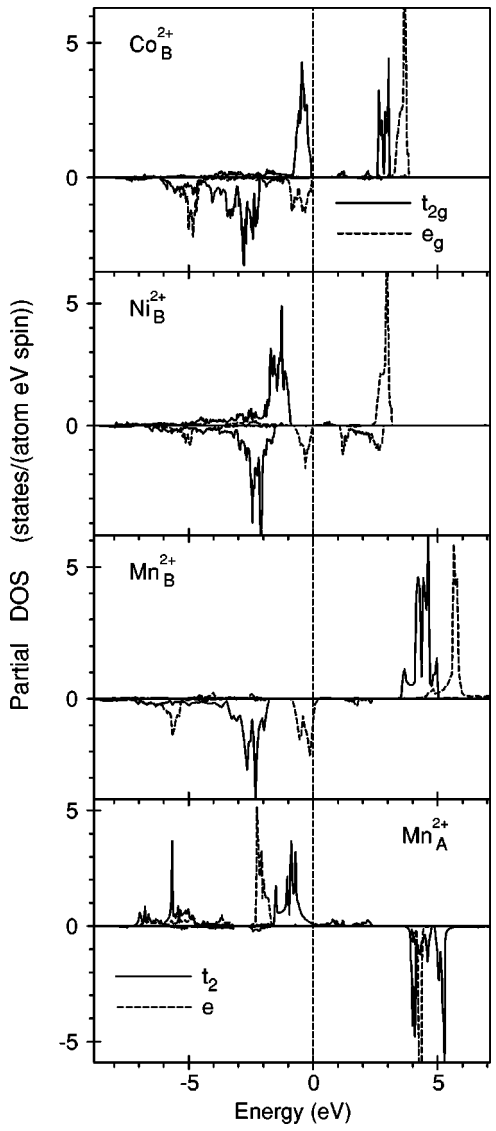

FIG. 7. The LSDA+*U* partial DOS of Co-, Ni-, and Mn-substituted Fe_3O_4.

B. Co-, Ni-, and Mn-substituted Fe_3O_4

We have calculated the electronic structure and XMCD spectra of Co-, Ni-, and Mn- substituted magnetite using the LSDA and LSDA+*U* methods.

The local symmetry of *A* and *B* sites in substituted magnetite is C_{2v} and C_{2h}, respectively. The crystal field causes the *d* orbitals to split into five singlets at each site: a_1', a_1'', b_1, a_2, and b_2 at the *A* site and a_{g1}, a_{g2}, a_{g3}, b_{g1}, and b_{g2} at the *B* site. We present in Fig. 7 the sum of DOS's of a_1'' and a_2 orbitals at site *A* (denoted as e) and the sum of a_1', b_1, and b_2 ones (t_2). Correspondingly, at the octahedral *B* site, we sum the DOS's of a_{g3} and b_{g2} (former e_g) and a_{g1}, a_{g2}, and b_{g1} (former t_{2g} orbitals).

Figure 7 shows the local partial density of states of Co^{2+}, Ni^{2+}, and Mn^{2+} ions in $Fe_A^{3+}[Co^{2+}Fe^{3+}]_B(O^{2-})_4$, $Fe_A^{3+}[Ni^{2+}Fe^{3+}]_B(O^{2-})_4$, $Fe_A^{3+}[Mn^{2+}Fe^{3+}]_B(O^{2-})_4$, and $Mn_A^{2+}[Fe_2^{3+}]_B(O^{2-})_4$ compounds, respectively. We do not show the energy distribution of local partial DOS for Fe^{3+} ions in these compounds because they are very similar to the ones in pure magnetite for both tetrahedral *A* and octahedral *B* sites (see Fig. 1).

In contrast to the LSDA, which produces the metallic solution in Co- and Ni-substituted magnetite, the LSDA+*U* gives an insulator in both cases. The energy gap of 0.63 eV in Co- substituted magnetite occurs between Co_B^{2+} $t_{2g\uparrow}$ (the top of valence band) and Fe_B^{3+} $t_{2g\uparrow}$ (bottom of empty conduction band) states at the Γ point. The gap in $NiFe_2O_4$ is equal to 0.99 eV. It appears between Ni_B^{2+} $e_{g\downarrow}$ and Fe_B^{3+} $t_{2g\uparrow}$ states. In this compound, Ni_B^{2+} t_{2g} orbitals are fully occupied.

It is known that orbital and spin magnetic moments are determined by the interplay of hybridization, exchange and Coulomb interactions, and crystal-field and spin-orbit couplings. The calculated spin M_s and orbital M_l magnetic moments on various atoms are given in Table I and compared with available experimental data.

TABLE I. The LSDA+U calculated spin M_s, orbital M_l and total M_{total} magnetic moments (in μ_B) in comparison with the calculated magnetic moments using sum rules (M_s^{sr} and M_l^{sr}) of Fe_3O_4 and Mn^{2+}, Co^{2+}, and Ni^{2+} substituted magnetite. The experimental value of the total magnetic moment of Fe_A^{3+} ion in Fe_3O_4 is equal to 3.82 μ_B (Ref. 83).

Compound	Ion	M_s	M_l	M_{total}	M_s^{sr}	M_l^{sr}
Fe_3O_4	Fe_A^{3+}	3.84	0.02	3.86	3.59	0.01
	Fe_B^{2+}	−3.54	−0.02	−3.56	−3.20	−0.01
	Fe_B^{3+}	−4.00	−0.02	−4.02	−3.65	−0.01
$Mn_A[Fe_2]_BO_4$	Mn_A^{3+}	4.08	−0.01	4.07	3.47	−0.02
	Fe_B^{2+}	−4.05	−0.05	−4.10	−3.42	−0.03
$Fe_A[MnFe]_BO_4$	Fe_A^{3+}	3.99	0.01	4.00	3.21	0.01
	Mn_B^{2+}	−4.47	−0.01	−4.48	−3.70	−0.07
	Fe_B^{3+}	−4.24	−0.15	−4.39	−3.81	−0.08
$Fe_A[CoFe]_BO_4$	Fe_A^{3+}	3.90	0.03	3.93	3.36	0.02
	Co_B^{2+}	−2.57	−0.01	−2.58	−2.16	−0.02
	Fe_B^{3+}	−4.04	−0.04	−4.08	−3.45	−0.04
$Fe_A[NiFe]_BO_4$	Fe_A^{3+}	3.99	0.02	4.01	3.51	0.03
	Ni_B^{2+}	−1.54	−0.27	−1.81	−1.32	−0.13
	Fe_B^{3+}	−4.09	−0.03	−4.12	−3.53	−0.05

Measurements indicate that the magnetic moment of an iron atom in Fe_3O_4 on the A site is much smaller than the 5.0μ_B of a pure Fe^{3+} ion.[83] This is an indication of strong hybridization between the 3d orbitals of Fe_A. As can be seen from Table I in all the compounds, the magnetic moments within the A and the B sublattices are ferromagnetically aligned while the two sublattices are antiferromagnetic with respect to each other. Due to band filling, there is a systematic reduction of the spin magnetic moment from Mn_B^{2+} to Ni_B^{2+} (Table I). Using the XMCD sum rules, the authors of Ref. 33 found for nickel in $NiFe_2O_4$ an orbital to spin magnetic-moment ratio $M_l/M_s = 0.27 \pm 0.07$. Our LSDA+U results give the ratio of 0.18 (Table I), which is in a reasonable agreement with the experimental data.[33]

The experimental measurements of the XMCD spectra at the Ni $L_{2,3}$ edge are reported in Ref. 33. The spectra were interpreted by atomic multiplet calculations for a 3d ground state including an octahedral crystal-field splitting.

Results of the LSDA+U circular dichroism calculations for the $L_{2,3}$ spectra of Fe and Ni are shown in Fig. 8 with the experimental data for the Ni $L_{2,3}$ edge.[33] As one can see, a rather pronounced XMCD is found. The XMCD spectrum is negative at the L_3 edge and positive at the L_2 edge at the Fe_B^{3+} and Ni_B^{2+} sites and vice versa for the Fe_A^{3+} ones. For Fe^{3+} ions, the dichroism at the L_3 edge is larger at tetrahedral A sites than at octahedral B ones. Due to their opposite signs and relative shift, the total Fe XMCD L_3 spectrum has a positive sharp peak with an additional negative shoulder on the high $h\nu$ side of the main peak. The same feature (with the opposite sign) is observed for the experimentally measured Ni^{2+} XMCD at the L_3 edge (Fig. 8) with a strong negative peak and a 2-eV positive shoulder of the main peak. The positive shoulder was attributed in Ref. 33 to a singlet spin-flip state that appears as a result of the transition of a spin-down core electron into an empty spin-up Ni d state. This transition becomes allowed since the selection rule $\Delta S = 0$ is broken by strong 2p spin-orbit interaction.

We should mention that the interpretation of the positive shoulder at 2 eV is controversial because the main peak of L_3 white line region suffers seriously from self-absorption and saturation artifacts due to its large absorption cross section. It is also very difficult to isolate the positive MCD signal of the satellite peak at 2 eV higher energy from negative MCD signal of the main peak.[34] Further investigations are necessary in order to clarify the nature of the positive shoulder at 2 eV.

The XMCD spectra of Co^{2+}-substituted magnetite have been reported for the Fe $M_{2,3}$ and Co $M_{2,3}$ core-absorption edges in Ref. 28. In Fig. 9, the experimentally measured Fe and Co $M_{2,3}$-XMCD spectra[28] in $CoFe_2O_4$ are compared to the theoretical ones calculated within the LSDA+U approach. Site-preference calculations[36] pointed out that Co^{2+} ions strongly prefer the octahedral B sites. The left column of Fig. 9 presents the theoretically calculated Fe and Co $M_{2,3}$ spectra with Co^{2+} ions occupying only octahedral B sites (theory 1) in comparison with the experimental measurements.[28] Two prominent negative minima b and d at 3 and 7 eV are derived from Fe_A^{3+} M_3 spectrum and Fe_B^{3+} M_2 one, respectively. The first positive maximum c at 4–5 eV is a sum of Fe_A^{3+} M_2 and Fe_B^{3+} M_3 spectra. The fine structure at 7–14 eV is from Co_B^{2+} ions. The LSDA calculations (not shown) produce a similar XMCD spectrum except that the intensity of the first minimum at 3 eV is strongly underestimated by the LSDA in comparison with the experiment.

Although, the LSDA+U theory with Co^{2+} ions occupying only octahedral B sites reasonably well describes all major features of the experimental spectrum, it fails to produce the positive shoulders a and f at 2 and 10 eV and also underestimates the intensity of two prominent minima b and d

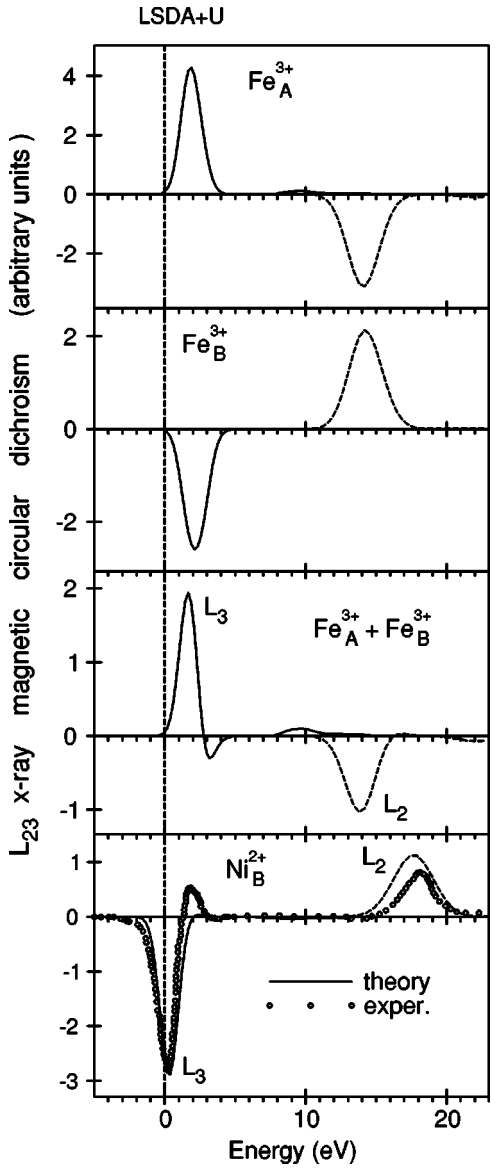

FIG. 8. The Fe and Ni $L_{2,3}$-XMCD spectra in $NiFe_2O_4$ calculated in the LSDA+U approximation in comparison with the experimental data (circles) (Ref. 33).

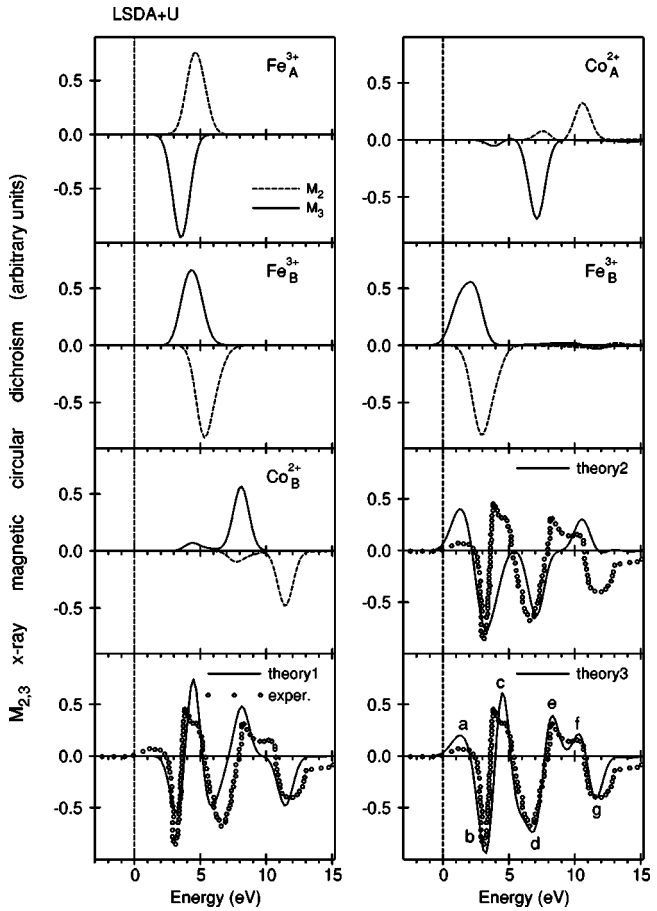

FIG. 9. The Co and Fe $M_{2,3}$-XMCD spectra in $CoFe_2O_4$ calculated in LSDA+U approximation in comparison with the experimental data (circles) (Ref. 28). Theory 1 presents $M_{2,3}$ XMCD spectrum in $Fe_A[CoFe]_BO_4$ compound, theory 2 for $Co_A[Fe_2]_BO_4$ compound, and theory 3 is a sum of 80% of the theory 1 and 20% of the theory 2.

at 3 and 7 eV. On the third panel from the top of the right column of Fig. 9, we present the theoretically calculated Fe and Co $M_{2,3}$ spectra with Co^{2+} ions occupying only tetrahedral *A* sites (theory 2). It is clearly seen that the shoulder *a* at 2 eV is derived from the Fe_B^{3+} M_3 spectrum and the peak *f* at 10 eV mostly comes from the Co_A^{2+} M_2 spectrum. Besides, the Fe_B^{3+} M_2 and Co_A^{2+} M_3 spectra contribute to the *b* and *d* minima, respectively. The best agreement between the theory and experiment can be achieved if we assume that 80% of the Co^{2+} occupy the octahedral *B* sites and 20% occupy tetrahedral *A* sites (see theory 3 on the fourth panel from the top of right column of Fig. 9).

The original idea in substituting Fe_B^{3+} ions by Co_B^{2+} ones was to simplify the XMCD spectra. It works for the $L_{2,3}$ edge, but for the $M_{2,3}$ edge, the result is opposite: instead of six XCMD spectra for Fe_3O_4 (see Fig. 5), we have ten $M_{2,3}$ spectra in Co substituted magnetite (from Fe_A^{3+}, Fe_B^{3+}, and Co_B^{2+} sites in $Fe_A[CoFe]_BO_4$ and from Fe_B^{3+} and Co_B^{2+} sites in $Co_A[Fe_2]_BO_4$) appear simultaneously in a rather small-energy range (Fig. 9).

Magnetic circular dichroism on the $2p$ and $3p$ core levels of Mn and Fe is reported for $Mn_{2/3}Zn_{1/3}Fe_2O_4$ ferrite in Ref. 35. Very large MCD signals were observed for both Mn and Fe with opposite sign for prominent features. As we mentioned above, the Mn^{2+} ion may occupy both the tetrahedral *A* and octahedral *B* sites with preference to the *A* sites.

Figure 10 presents the experimentally measured Mn $L_{2,3}$-XMCD spectra[35] in $Mn_{2/3}Zn_{1/3}Fe_2O_4$ in comparison with the theoretical calculations within the LSDA+U approach. The dichroism at the L_3 edge is much larger for Mn^{2+} ions at tetrahedral *A* sites than at *B* ones. The prominent negative minimum of L_3 XMCD spectrum at around 4 eV is almost completely derived from Mn^{2+} ions at tetrahedral *A* sites. The positive shoulder at 6 eV is due to Mn_B^{2+} ions at octahedral *B* sites. The best agreement between the theory and experiment can be achieved if we assume that 30% of the Mn^{2+} ions occupy the octahedral *B* sites and

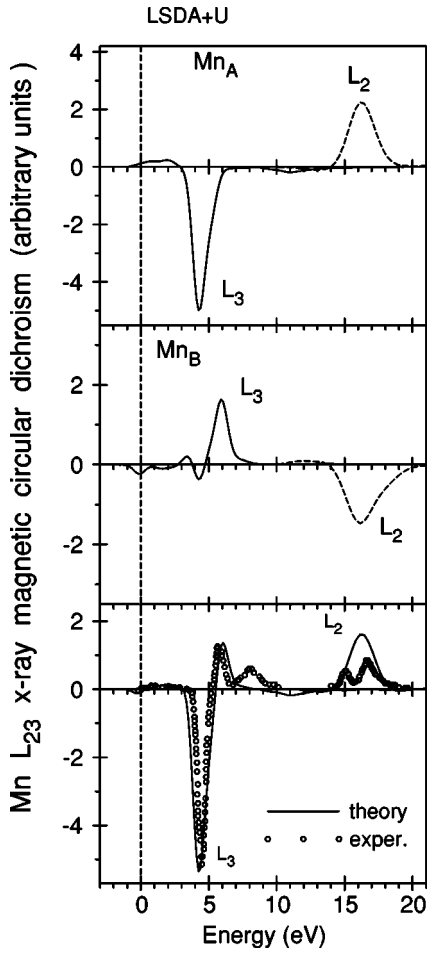

FIG. 10. The Mn $L_{2,3}$-XMCD spectra in $MnFe_2O_4$ calculated in the LSDA+U approximation in comparison with the experimental data (circles) (Ref. 35).

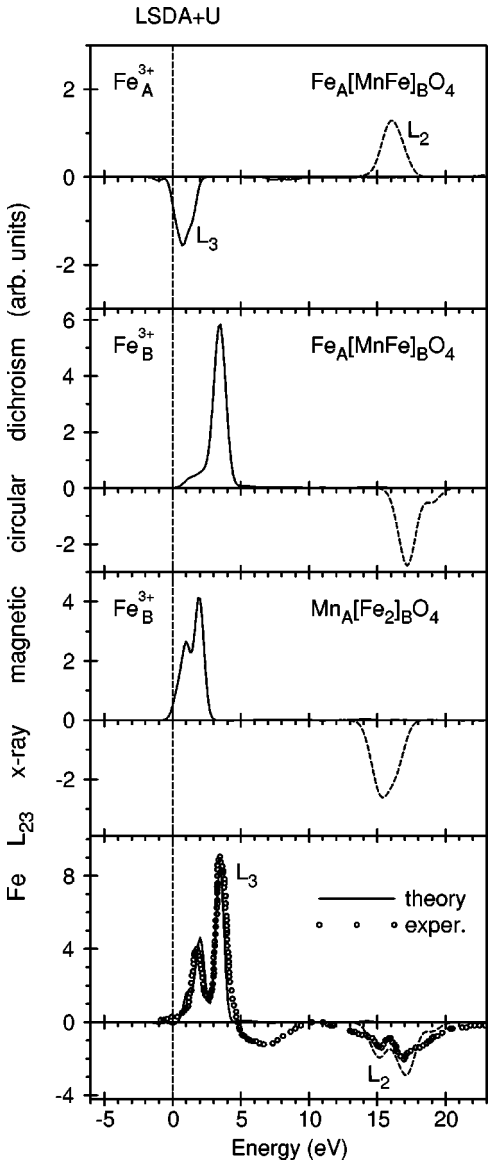

FIG. 11. The Fe $L_{2,3}$-XMCD spectra of $MnFe_2O_4$ calculated with the LSDA+U approximation in comparison with the experimental data (circles) (Ref. 35).

70% occupy tetrahedral A sites (see theory on the third panel from the top of Fig. 10). Even with this Mn-ion distribution, theory is not able to produce the second positive shoulder at 8 eV as well as a double structure at the L_2 edge.

In Fig. 11, the experimentally measured Fe $L_{2,3}$-XMCD spectra[35] in $Mn_{2/3}Zn_{1/3}Fe_2O_4$ are compared to the theoretical calculations. Theory correctly produces a double-peak structure at the L_3 and L_2 edges, although it was not able to produce additional negative component at the high-energy side of the main double peak at 5–9 eV at the L_3 edge.

If we assume that Mn^{2+} can occupy either the tetrahedral A or octahedral B sites, there are three different types of Fe^{3+}-ion sites depending on which site is occupied by the Mn^{2+} ions (Fig. 11). If Mn^{2+} ions occupy A sites, there is only one type of Fe^{3+} ion at the B sites with a positive double-peak structure at the L_3 edge and negative dichroism at the L_2 edge. If Mn^{2+} ions occupy octahedral B sites, there are two types of Fe^{3+} ions at the A and B sites. These two iron ions are antiferromagnetically ordered and, hence, have opposite signs in the magnetic dichroism. The prominent positive maximum at around 3.5 eV at the L_3 edge is derived mostly from the Fe_B^{3+} ions with Mn^{2+} ions occupying octahedral B sites. The low-energy peak at 2 eV is due to the Fe_B^{3+} ions with Mn^{2+} ions occupying tetrahedral A sites, this peak is partly compensated by a negative dichroic signal from the Fe_A^{3+} ions with Mn^{2+} ions at the B sites. The final theoretical spectrum on the fourth panel from the top of Fig. 11 is obtained from a sum of 70% Fe $L_{2,3}$ spectra from $Mn_A[Fe_2]_BO_4$ and 30% from $Fe_A[MnFe]_BO_4$.

In Fig. 12, the experimentally measured Mn and Fe $M_{2,3}$-XMCD spectra[35] in $Mn_{2/3}Zn_{1/3}Fe_2O_4$ are compared to the theoretical ones calculated within the LSDA+U approach. As in the case of Co-substituted Fe_3O_4 (Fig. 9), Mn-substituted magnetite has also ten $M_{2,3}$ spectra at the $M_{2,3}$ edge (from Mn_B^{2+} and Fe_B^{3+} sites in the $Mn_A[Fe_2]_BO_4$ compound and from Fe_A^{3+}, Fe_B^{3+}, and Mn_B^{2+} sites in the $Fe_A[MnFe]_BO_4$ compound) (Fig. 12). The best agreement between the theory and experiment can be achieved if we assume that 70% of the Mn^{2+} occupy the tetrahedral A sites

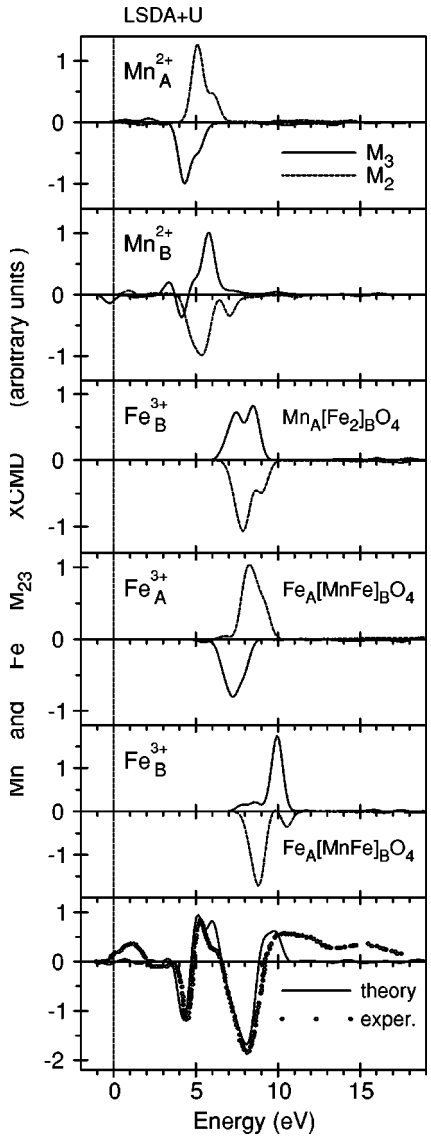

FIG. 12. The Mn $M_{2,3}$-XMCD spectra in $MnFe_2O_4$ calculated in the LSDA+U approximation in comparison with the experimental data (circles) (Ref. 35).

and 30% occupy octahedral B sites (see theory on the sixth panel from the top of Fig. 12). In this case, the agreement between theory and experiment is quite good except for being low at 0–2 eV and high in energy above the 11 eV tails, where the theory gives smaller dichroism in comparison with the experimental data. The prominent negative minimum at around the 4 eV is derived mostly from the Mn^{2+} M_3 spectrum at tetrahedral A site. The positive double peak at 5–6.5 eV is a superposition of Mn_A^{2+} M_2 and Mn_B^{2+} M_3 spectra suppressed by a negative signal from the Mn_B^{2+} M_2 spectrum. The features above 7 eV are completely derived from Fe ions on both sublattices.

C. XMCD sum rules

Concurrent with the x-ray magnetic circular dichroism experimental developments, some important magneto-optical sum rules have been derived in recent years. A sum rule was developed by van der Laan and Thole[84] relating the integrated signals over the spin-orbit split-core edges of the unpolarized XAS to the expectation value of the ground-state spin-orbit operator. Later Thole *et al.*[85] and Carra *et al.*[86] derived sum rules to relate the integrated signals over the spin-orbit split-core edges of the circular dichroism to ground-state orbital and spin magnetic moments by using an ion model for atoms. In the case of solids, the corresponding XMCD sum rules were proposed by Ankudinov and Rehr,[87] Strange and Gyorffy,[88] and Guo.[89] Sum rules for x-ray magnetic scattering were derived by Luo *et al.*[90]

For the $L_{2,3}$ edges, the l_z sum rule can be written as

$$\langle l_z\rangle = -n_h \frac{4\int_{L_3+L_2} d\omega(\mu_+ - \mu_-)}{3\int_{L_3+L_2} d\omega(\mu_+ + \mu_-)}, \tag{5}$$

where n_h is the number of holes in the d band $n_h = 10 - n_{3d}$, $\langle l_z\rangle$ is the average of the magnetic quantum number of the orbital angular momentum. The integration is taken over the whole $2p$ absorption region. The s_z sum rule is written as

$$\langle s_z\rangle + \frac{7}{2}\langle t_z\rangle = -n_h \frac{6\int_{L_3} d\omega(\mu_+ - \mu_-) - 4\int_{L_2} d\omega(\mu_+ - \mu_-)}{\int_{L_3+L_2} d\omega(\mu_+ + \mu_-)}, \tag{6}$$

where t_z is the z component of the magnetic dipole operator $\mathbf{t} = \mathbf{s} - 3\mathbf{r}(\mathbf{r}\cdot\mathbf{s})/|\mathbf{r}|^2$, which accounts for the asphericity of the spin moment. The integration $\int_{L_3}$ ($\int_{L_2}$) is taken only over the $2p_{3/2}$ ($2p_{1/2}$) absorption region. In these equations, we have replaced the linear polarized spectra μ_0 by $[\mu_+(\omega) + \mu_-(\omega)]/2$.

Because of the significant implications of the sum rules, numerous experimental and theoretical studies aimed at investigating their validity for itinerant magnetic systems have been reported, but with widely different conclusions. The claimed adequacy of the sum rules varies from very good (within 5% agreement) to very poor (up to 50% discrepancy).[2,85,86,91–96] This lack of a consensus may have several origins. For example, on the theoretical side, it has been demonstrated by circularly polarized $2p$ resonant photoemission measurements of Ni that both the band-structure effects and electron-electron correlations are needed to satisfactorily account for the observed MCD spectra.[97] However, it is extremely difficult to include both of them in a single theoretical framework. Besides, the XAS as well as XMCD spectra can be strongly affected (especially for the early transition metals) by the interaction of the excited electron with the created core hole.[98] On the experimental side, the indirect x-ray absorption techniques, i.e., the total electron and fluorescence yield methods, are known to suffer from saturation

and self-absorption effects that are very difficult to correct for.[93] The total electron yield method can be sensitive to the varying applied magnetic field, changing the electron detecting efficiency, or, equivalently, the sample photocurrent. The fluorescence yield method is insensitive to the applied field, but the yield is intrinsically not proportional to the absorption cross section because the radiative to nonradiative relative core-hole decay probability depends strongly on the symmetry and spin polarization of the XAS final states.[2]

To derive the sum rules, a great number of assumptions had to be made.[39] For $L_{2,3}$, they are (1) ignore the exchange splitting for the core levels; (2) replace the interaction operator $\boldsymbol{\alpha}\cdot\mathbf{a}_\lambda$ in Eq. (1) by $\boldsymbol{\nabla}\cdot\mathbf{a}_\lambda$; (3) ignore the asphericity of the core states; (4) ignore $p\rightarrow s$ transitions; (5) ignore the difference of $d_{3/2}$ and $d_{5/2}$ radial wave functions; (6) ignore the interatomic hybridization, which is reflected on the nontreatment of any energy dependence of the radial matrix elements. The three last points are the most important. The problem of the ignoring of the $p\rightarrow s$ transitions was considered by Wu and Freeman[96] in the case of pure Fe, Co, Ni, and their surfaces. They demonstrate that the application of the spin sum rule results in an error up to 52% for the Ni(001) surface. On the other hand, the orbital sum rule is affected much less.

Taking into account all the above-mentioned problems, it is interesting to compare the spin and orbital magnetic moments obtained from the theoretically calculated XAS and XMCD spectra through the sum rules [Eqs. (5) and (6)] with the directly calculated LSDA$+U$ values. In this case, we at least avoid all the experimental problems.

Table I shows direct and sum rule derived spin and orbital magnetic moments from the theoretical XMCD $L_{2,3}$ spectra. We neglected in our calculations the term $\langle t_z\rangle$ in Eq. (6). It was shown that this term is negligible for cubic systems.[39,58] The number of the $3d$ electrons is calculated by integrating the element and lj projected density of states inside each atomic sphere. The values $n_{3d}=5.834$, 6.599, and 6.312 for Fe_A^{3+}, Fe_B^{2+}, and Fe_B^{3+} ions in Fe_3O_4; 4.978 and 6.255 for Mn_A^{2+} and Fe_B^{3+} in $Mn_A[Fe_2]_BO_4$; 5.987, 5.669, and 6.370 for Fe_A^{3+}, Mn_B^{2+}, and Fe_B^{3+} in $Fe_A[MnFe]_BO_4$; 5.795, 7.658, and 6.240 for Fe_A^{3+},Co_B^{2+}, and Fe_B^{3+} in $Fe_A[CoFe]_BO_4$, 5.796, 7.765, and 6.246 for Fe_A^{3+}, Ni_B^{2+}, and Fe_B^{3+} in $Fe_A[NiFe]_BO_4$, respectively.

As can be seen from Table I, the general trend of the sum-rule results is in a reasonable agreement with the LSDA$+U$ calculated spin and orbital magnetic moments for both the tetrahedral and octahedral sites. The orbital magnetic moments at tetrahedral sites agree well with the direct calculations, but the orbital moments at octahedral sites are overestimated for Mn_B^{2+} ions in $Fe_A[MnFe]_BO_4$ and for Fe_B^{3+} ions in $Fe_A[NiFe]_BO_4$ and underestimated for Fe_B^{3+} ions in $Fe_A[MnFe]_BO_4$ and for Ni_B^{2+} ions in $Fe_A[NiFe]_BO_4$. The spin magnetic moments deduced from the theoretical XMCD spectra are systematically underestimated for all the compounds. The disagreement at tetrahedral sites varies from 7% for Fe_A^{3+} ions in Fe_3O_4 up to 24% for Fe_A^{3+} ions in $Fe_A[MnFe]_BO_4$, whereas the correspondent disagreement for octahedral B sites varies from 10% for Fe_B^{2+} ions in Fe_3O_4 up to 21% for Mn_B^{2+} ions in $Fe_A[MnFe]_BO_4$. Such behavior arises probably because the sum rules ignore the p to s transitions, which play an essential role in the formation of the spin magnetic moments in transition metals. Thus, first principles determinations of both the XMCD spectra and ground-state properties (M_l and M_s) are probably required for quantitative interpretation of the experimental results.

IV. SUMMARY

We have studied by means of an *ab initio* fully relativistic spin-polarized Dirac linear muffin-tin orbital (LMTO) method combined with the LSDA$+U$ approach the electronic structure and the x-ray magnetic circular dichroism for Fe_3O_4 and Mn-, Co-, or Ni- substituted Fe_3O_4.

The orbital and spin magnetic moments of the compounds have been evaluated from first-principles electronic-structure calculations.

We have calculated the x-ray absorption spectra as well as the x-ray circular magnetic dichroism at the K $L_{2,3}$ and $M_{2,3}$ edges for transition-metal sites. Due to the small-exchange splitting of the initial $1s$-core states, only the exchange and spin-orbit couplings of the final $4p$ states is responsible for the observed dichroism at the K edge. We demonstrated that the XMCD K-spectrum reflects the orbital polarization of the p states in differential form [the $dm_{l=1}(E)$ function].

The XMCD spectra of transition metals for the $L_{2,3}$ edge are mostly determined by the strength of the SO coupling of the initial $2p$ core states and spin-polarization of the final empty $3d_{3/2,5/2}$ states, while the exchange splitting of the $2p$ core states as well as SO coupling of the $3d$ valence states are of minor importance. The LSDA$+U$ calculated $L_{2,3}$ XMCD spectra of Fe_3O_4 are in good agreement with the experimental measurements, while the LSDA calculations underestimate the intensity of the first negative minimum. The theoretical analysis shows that two prominent negative minima of Fe L_3-XMCD spectrum are derived from iron ions at octahedral B sites. The major positive maximum is from Fe_A^{3+} ions.

The spin-orbit splitting of the $3p$-core level is of one order of magnitude smaller than for the $2p$ level in Fe_3O_4. As a result, the magnetic dichroism at the $M_{2,3}$ edge is smaller than at the $L_{2,3}$ edge. Besides, the M_2 and the M_3 spectra are strongly overlapped and the M_3 spectrum contributes to some extent to the structure of the total $M_{2,3}$ spectrum in the region of the M_2 edge. In Fe_3O_4, the magnetic moments within the A and the B sublattices are ferromagnetically aligned, while the two sublattices are antiferromagnetic with respect to each other. The XMCD spectra are positive at the M_3 edge and negative at the M_2 edge at the tetrahedral A sites and vice versa for the octahedral B ones. The LSDA$+U$ calculations reasonably well produce overall features of the experimentally measured Fe $M_{2,3}$-XMCD spectrum.

Due to the small-energy differences of Co and Fe $3p$ core states, ten $M_{2,3}$ spectra (from Fe_A^{3+}, Fe_B^{3+}, Co_B^{2+}, and Co_A^{2+} sites) appear simultaneously in a rather small-energy range

producing a very complicated spectrum. We found a reasonable agreement with the experimental results for Fe and Co $M_{2,3}$-XMCD spectra in $CoFe_2O_4$ by assuming that Co^{2+} ions occupy both the tetrahedral *A* and octahedral *B* sites.

The LSDA+*U* theory describes well all the prominent features of the magnetic circular dichroism on the $2p$ and $3p$ core levels of $Mn_{2/3}Zn_{1/3}Fe_2O_4$ with the assumption that 70% Mn^{2+} occupy the tetrahedral *A* and 30% octahedral *B* sites.

Indeed, our work shows how sensitive the XMCD spectra can be for the same magnetic ions on different sites, and by comparing the experimental spectra with careful theoretical analysis a quantitative estimate for site occupancy may be easily obtained.

ACKNOWLEDGMENTS

This work was carried out at the Ames Laboratory, which is operated for the US Department of Energy by Iowa State University under Contract No. W-7405-82. This work was supported by the Director for Energy Research, Office of Basic Energy Sciences of the U.S. Department of Energy. V.N. Antonov gratefully acknowledges the hospitality during his stay at Ames Laboratory.

*Email address: antonov@ameslab.gov; anton@imp.kiev.ua; Permanent address: Institute of Metal Physics, Vernadskii Street, 03142 Kiev, Ukraine.

[1] A short modern history of XMD can be found at http://psi-k.dl.ac.uk/psi-k/hp.html

[2] C.T. Chen, Y.U. Idzerda, H.-J. Lin, N.V. Smith, G. Meigs, E. Chaban, G.H. Ho, E. Pellegrin, and F. Sette, Phys. Rev. Lett. **75**, 152 (1995).

[3] C.M. Schneider, K. Holldack, M. Kinzler, M. Grunze, H.P. Oepen, F. Schäfers, H. Petersen, K. Meinel, and J. Kirschner, Appl. Phys. Lett. **63**, 2432 (1993).

[4] K. Holldack, F. Schäfers, T. Kachel, and J. Packe, Rev. Sci. Instrum. **67**, 2485 (1996).

[5] E.J. Verwey and P. Haayman, Physica (Amsterdam) **8**, 979 (1941).

[6] See the papers at the Cavendish Meeting, September 1979; N. F. Mott, Philos. Mag. B **42**, 327 (1980).

[7] B.A. Calhoun, Phys. Rev. **94**, 1577 (1954); P.A. Miles, W.B. Westphal, and A. von Hippel, Rev. Mod. Phys. **29**, 279 (1957); M. Motsui, S. Todo, and S. Chikazumi, J. Phys. Soc. Jpn. **42**, 1517 (1977).

[8] E.J. Verwey, P. Haayman, and F. Romrin, J. Chem. Phys. **15**, 181 (1947).

[9] C. Bonnele, Ann. Phys. (Paris) **1**, 439 (1966).

[10] Y. Ma, P.D. Johnson, N. Wassdahl, J. Guo, P. Skytt, J. Nordgren, S.D. Keven, J.E. Rubensson, T. Böske, and W. Eberhardt, Phys. Rev. B **48**, 2109 (1993).

[11] S.G. Bishop and P.C. Kemeny, Solid State Commun. **15**, 1877 (1974).

[12] A.J.M. Kuipers and V.A.M. Brabers, Phys. Rev. B **14**, 1401 (1976); Phys. Rev. B **20**, 594 (1979).

[13] A. Chainani, T. Yokoya, T. Morimoto, T. Takahashi, and S. Todo, Phys. Rev. B **51**, 17 976 (1995).

[14] S.F. Alvarado, W. Eib, F. Meier, D.T. Pierce, K. Sattler, H.C. Siegmann, and J.P. Remeika, Phys. Rev. Lett. **34**, 319 (1975); S.F. Alvarado, M. Erbudak, and P. Munz, Phys. Rev. B **14**, 2740 (1976).

[15] K. Siratory, S. Suga, M. Taniguchi, K. Soda, S. Kimura, and A. Yanase, J. Phys. Soc. Jpn. **55**, 690 (1986).

[16] T. Schedel-Niedring, W. Weiss, and R. Schlögl, Phys. Rev. B **52**, 17 449 (1995).

[17] M. Sancrotti, F. Ciccacci, M. Finazzi, E. Vescovo, and S.F. Alvarado, Z. Phys. B: Condens. Matter **84**, 243 (1991).

[18] Y.Q. Cai, M. Ritter, W. Weis, and A.M. Bradshaw, Phys. Rev. B **58**, 5042 (1998).

[19] J.H. Park, L.H. Tjeng, J.W. Allen, P. Metcalf, and C.T. Chen, Phys. Rev. B **55**, 12 813 (1997).

[20] A. Schlegel, S.F. Alvarado, and P. Wachter, J. Phys. C **12**, 1157 (1979).

[21] S.K. Park, T. Ishikawa, and Y. Tokura, Phys. Rev. B **58**, 3717 (1998).

[22] X. Zhang, J. Schoenes, W. Reim, and P. Wachter, J. Phys. C **16**, 6055 (1983).

[23] W.F.J. Fontijn, P.J. van der Zaag, M.A.C. Deviller, V.A.M. Brabers, and R. Metselaar, Phys. Rev. B **56**, 5432 (1997).

[24] Z. Simsa, H. LeGall, and P. Siroky, Phys. Status Solidi B **100**, 666 (1980); Z. Simsa, P. Siroky, J. Kolacek, and V.A. Brabers, J. Magn. Magn. Mater. **15-18**, 775 (1980).

[25] X. Zhang, J. Schoenes, and P. Wachter, Solid State Commun. **39**, 189 (1981).

[26] S. Visnovsky, V. Prosser, R. Krishnan, V. Parizek, K. Nitsch, and L. Svobodova, IEEE Trans. Magn. **MAG-17**, 3205 (1981).

[27] P. Kuiper, B.G. Searle, L.C. Duda, R.M. Wolf, and P.J. van der Zaag, J. Electron Spectrosc. Relat. Phenom. **86**, 107 (1977).

[28] T. Koide, T. Shidara, K. Yamaguchi, A. Fujimori, H. Fukutani, N. Kimizuka, and S. Kimura, J. Electr. Spectr. **78**, 275 (1996).

[29] A. Yanase and K. Siratory, J. Phys. Soc. Jpn. **53**, 312 (1984).

[30] Z. Zhang and S. Satpathy, Phys. Rev. B **44**, 13 319 (1991).

[31] V.I. Anisimov, I.S. Elfimov, N. Hamada, and K. Terakura, Phys. Rev. B **54**, 4387 (1996).

[32] V.N. Antonov, B.N. Harmon, V.P. Antropov, A.Ya. Perlov, and A.N. Yaresko, Phys. Rev. B **64**, 134410 (2001).

[33] G. van der Laan, C.M.B. Henderson, R.A.D. Pattrick, S.S. Dhesi, P.F. Schofield, E. Dudzik, and D.J. Vaughan, Phys. Rev. B **59**, 4314 (1999).

[34] W.F. Pong, Y.K. Chang, M.H. Su, P.K. Tseng, H.J. Lin, G.H. Ho, K.L. Tsang, and C.T. Chen, Phys. Rev. B **55**, 11 409 (1997).

[35] S. Suga and S. Imada, J. Electr. Spectr. **92**, 1 (1999).

[36] J. Smit and H. P. J. Wijn, *Ferrite* (Wiley-Interscience, New York, 1959).

[37] N.S. Satya Murthy, M.G. Natera, S.I. Youssef, R.J. Begum, and C.M. Srivastava, Phys. Rev. B **181**, 969 (1969).

[38] V.G. Harris, N.C. Koon, C.M. Williams, O. Zhang, M. Abe, and J.P. Kirkland, Appl. Phys. Lett. **68**, 2082 (1996).

[39] H. Ebert, Rep. Prog. Phys. **59**, 1665 (1996).

[40] J.P. Hannon, G.T. Trammel, M. Blume, and D. Gibbs, Phys. Rev. Lett. **61**, 1245 (1988).

[41] S. W. Lovsey and S. P. Collins, *X-Ray Scattering and Absorption in Magnetic Materials* (Oxford University Press, Oxford, New York, 1996).

[42] J.B. Kortight and S.-K. Kim, Phys. Rev. B **62**, 12 216 (2000).

[43] W.H. Kleiner, Phys. Rev. **142**, 318 (1966).

[44] F.U. Hillebrecht, C. Roth, H.B. Rose, W.G. Park, E. Kisker, and

Kirschner, Phys. Rev. B **55**, 2594 (1997).
[45] J.G. Menchero, Phys. Rev. B **57**, 993 (1998).
[46] G. van der Laan, J. Magn. Magn. Mater. **148**, 53 (1995).
[47] G. van der Laan, J. Electron Spectrosc. Relat. Phenom. **86**, 41 (1997).
[48] G. van der Laan, J. Phys.: Condens. Matter **9**, L259 (1997).
[49] G. van der Laan, Phys. Rev. B **57**, 5250 (1998).
[50] J.G. Menchero, Phys. Rev. B **57**, 1001 (1998).
[51] A. Fanelsa, R. Schellenberg, F.U. Hillebrecht, E. Kisker, J.G. Menchero, A.P. Kaduwela, C.S. Fadley, and M.A. Van Hove, Phys. Rev. B **54**, 17 962 (1996).
[52] J.G. Menchero, C.S. Fadley, G. Panaccione, F. Sirotti, G.J. Henk, and R. Feder, Phys. Rev. B **55**, 11 476 (1997).
[53] J.G. Menchero, Phys. Rev. B **55**, 5505 (1997).
[54] R. Schellenberg, E. Kisker, A. Fanelsa, F.U. Hillebrecht, J.G. Menchero, A.P. Kaduwela, C.S. Fadley, and M.A.V. Hove, Phys. Rev. B **57**, 14 310 (1998).
[55] H. Ebert, L. Baumgarten, C.M. Schneider, and J. Kirschner, Phys. Rev. B **44**, 4406 (1991).
[56] H. Ebert and G.-Y. Guo, J. Magn. Magn. Mater. **148**, 178 (1995).
[57] G.Y. Guo, H. Ebert, W.M. Temmerman, and P.J. Durham, Phys. Rev. B **50**, 3861 (1994).
[58] E. Tamura, G.D. Waddill, J.G. Tobin, and P.A. Sterne, Phys. Rev. Lett. **73**, 1533 (1994).
[59] A.H. MacDonald and S.H. Vosko, J. Phys. C **12**, 2977 (1979).
[60] O.K. Andersen, Phys. Rev. B **12**, 3060 (1977).
[61] D.D. Koelling and B.N. Harmon, J. Phys. C **10**, 3107 (1977).
[62] H. Ebert, Phys. Rev. B **38**, 9390 (1988).
[63] I.V. Solovyev, A.B. Shik, V.P. Antropov, A.I. Liechtenstein, V.A. Gubanov, and O.K. Andersen, Sov. Phys. Solid State **31**, 1285 (1989).
[64] H. Ebert, H. Freyer, A. Vernes, and G.-Y. Guo, Phys. Rev. B **53**, 7721 (1996).
[65] V.N. Antonov, A.I. Bagljuk, A.Ya. Perlov, V.V. Nemoshkalenko, Vl.N. Antonov, O.K. Andersen, and O. Jepsen, Low Temp. Phys. **19**, 689 (1993); **19**, 494 (1993).
[66] V.V. Nemoshkalenko, V.N. Antonov, Vl.N. Antonov, W. John, H. Wonn, and P. Ziesche, Phys. Status Solidi B **111**, 11 (1982); V.V. Nemoshkalenko, V.N. Antonov, Vl.N. Antonov, and W. John, *ibid.* **93**, 575 (1979).
[67] U. von Barth and L.A. Hedin, J. Phys. C **5**, 1629 (1972).
[68] V. V. Nemoshkalenko and V. N. Antonov, *Computational Methods in Solid State Physics* (Gordon and Breach, London, 1998).
[69] P.E. Blöchl, O. Jepsen, and O.K. Andersen, Phys. Rev. B **49**, 16 223 (1994).
[70] J. C. Fuggle and J. E. Inglesfield, *Unoccupied Electronic States. Topics in Applied Physics* (Springer, New York, 1992), Vol. 69.
[71] V.I. Anisimov, J. Zaanen, and O.K. Andersen, Phys. Rev. B **44**, 943 (1991).
[72] J. F. Herbst and J. W. Wilkins, in *Handbook of the Physics and Chemistry of Rare Earths*, edited by K. A. Gschneidner, L. Eyring, and S. Hüfner (North-Holland, Amsterdam, 1987), Vol. 10, p. 321.
[73] P.H. Dederics, S. Blügel, R. Zeller, and H. Akai, Phys. Rev. Lett. **53**, 2512 (1984).
[74] V.I. Anisimov and O. Gunnarsson, Phys. Rev. B **43**, 7570 (1991).
[75] V.N. Antonov, A.N. Yaresko, A.Ya. Perlov, P. Thalmeier, P. Fulde, P.M. Oppeneer, and H. Eschrig, Phys. Rev. B **58**, 9752 (1998).
[76] A. N. Yaresko, V. N. Antonov, and P. Fulde, Phys. Rev. B (to be published).
[77] I.V. Solovyev, A.I. Liechtenstein, and K. Terakura, Phys. Rev. Lett. **80**, 5758 (1998).
[78] P. Carra, B.N. Harmon, B.T. Thole, M. Altarelli, and G. A Sawatzky, Phys. Rev. Lett. **66**, 2495 (1991).
[79] H.J. Gotsis and P. Strange, J. Phys.: Condens. Matter **6**, 1409 (1994).
[80] M. S. S. Brooks and B. Johansson, in *Spin-Orbit Influenced Spectroscopies*, edited by H. Ebert and G. Schultz (Springer, Heidelberg, 1996), p. 211.
[81] L. Uba, S. Uba, V.N. Antonov, T. Ślęzak, J. Korecki, and A.N. Yaresko, Phys. Rev. B **63**, 013 731 (2000).
[82] J.H. van Vleck, *Electric and Magnetic Susceptibilities* (Oxford University Press, Oxford, New York, 1932).
[83] V.C. Rakhecha and N.S. Satya Murthy, J. Phys. C **11**, 4389 (1978).
[84] G. van der Laan and B.T. Thole, Phys. Rev. B **38**, 3158 (1988).
[85] B.T. Thole, P. Carra, F. Sette, and G. van der Laan, Phys. Rev. Lett. **68**, 1943 (1992); G. van der Laan and B.T. Thole, Phys. Rev. B **53**, 14 458 (1996); G. van der Laan, *ibid.* **57**, 112 (1998).
[86] P. Carra, B.T. Thole, M. Altarelli, and X. Wang, Phys. Rev. Lett. **70**, 694 (1993).
[87] A. Ankudinov and J.J. Rehr, Phys. Rev. B **51**, 1282 (1995).
[88] P. Strange and B.L. Gyorffy, Phys. Rev. B **52**, R13 091 (1995).
[89] G.Y. Guo, Phys. Rev. B **57**, 10 295 (1998).
[90] J. Luo, G.T. Trammell, and J.P. Hannon, Phys. Rev. Lett. **71**, 287 (1993).
[91] Y. Wu, J. Stöhr, B.D. Hermsmeier, M.G. Sumant, and D. Weller, Phys. Rev. Lett. **69**, 2307 (1992).
[92] J. Vogel and M. Sacchi, Phys. Rev. B **49**, 3230 (1994).
[93] T. Böske, W. Clemens, C. Carbone, and W. Eberhardt, Phys. Rev. B **49**, 3230 (1994).
[94] W.L. O'Brain, B.P. Tonner, G.R. Harp, and S.S.P. Parkin, J. Appl. Phys. **76**, 6462 (1994); W.L. O'Brain and B.P. Tonner, Phys. Rev. B **50**, 12 672 (1994).
[95] G. Y. Gao, H. Ebert, W. M. Temmerman, and P. J. Durham, in *Metallic Alloy: Experimental and Theoretical Perspective*, edited by J. S. Faulkner (Kluwer Academic, Dordrecht, 1993).
[96] R. Wu and A.J. Freeman, Phys. Rev. Lett. **73**, 1994 (1994).
[97] L.H. Tjeng, C. T. Chen, P. Rudolf, G. Meigs, G. van der Laan, and B. T. Thole, Phys. Rev. B **48**, 13 378 (1994).
[98] J. Zaanen, G.A. Sawatzky, J. Fink, W. Speier, and J.C. Fuggle, Phys. Rev. B **37**, 4905 (1985); J. Schwitalla and H. Ebert, Phys. Rev. Lett. **80**, 4586 (1998).